Organic Electronics 45 (2017) 74–80

Contents lists available at ScienceDirect

Organic Electronics

journal homepage: www.elsevier.com/locate/orgel

Vertically-oriented few-layer graphene supported by silicon microchannel plates as a counter electrode in dye-sensitized solar cells

Fengjuan Miao [a, *, 1], Rui Miao [a, 1], Bairui Tao [a, b, *], Zaishun Jin [d], Jianbo Yu [b], Paul K. Chu [c], Fang Liu [d], Lili Shao [d], Chunmei Li [d], Xiaodong Zhu [d]

[a] College of Communications and Electronics Engineering, Qiqihar University, Heilongjiang, 161006, China
[b] Modern Education Technology Center, Qiqihar University, Heilongjiang, 161006, China
[c] Department of Physics and Materials Sciences, City University of Hong Kong, Tat Chee Avenue, Kowloon, Hong Kong, China
[d] Mudanjiang Medical College, Heilongjiang, 157011, China

ARTICLE INFO

Article history:
Received 13 January 2017
Received in revised form
24 February 2017
Accepted 26 February 2017
Available online 27 February 2017

Keywords:
Graphene/Si-MCP
Dye-sensitized solar cells
Annealing temperature

ABSTRACT

Vertically-oriented few-layer graphene supported by silicon microchannel plates annealed at different temperatures are used in dye-sensitized solar cells (DSSCs). The structure, morphology, and electrochemical characteristics are determined by AFM, SEM, XPS, cyclic voltammetry, electrochemical impedance spectroscopy, and photocurrent density-voltage curves. The graphene/Si-MCP fabricated by electrochemical exfoliation delivers enhanced power conversion efficiency in DSSC and the materials annealed under ambient conditions at 300 °C show the best results due to the smaller oxygen concentration in graphene and larger electrical conductance. Owing to the microelectronics-compatible fabrication process and excellent properties of the device, the counter electrode has large potential in high-performance silicon-based monolithic DSSCs.

1. Introduction

Dye-sensitized solar cells (DSSCs) have aroused tremendous interest due to the low cost, easy fabrication, and high efficiency [1–3]. A typical DSSC consists of three parts, a dye-sensitized TiO_2 photoanode, an electrolyte containing a redox couple (I^-/I_3^-), and a counter electrode. During operation, I^- in the electrolyte is oxidized on the TiO_2 photoanode under light illumination and I_3^- is reduced on the counter electrode. The counter electrode plays an importance role which determines the reduction rate of the I^-/I_3^- redox pair and enables the dye to return from an excited state to the ground state [4,5]. Since the counter electrode should have high reduction activity, platinum (Pt) is typically used due to its high catalytic activity [6]. However, the high cost and scarcity being a noble metal hamper large-scale industrial application and so it is desirable to identify cheaper and more abundant materials with high catalytic activity to substitute for Pt.

Graphene, a one-atom-thick hexagonal mesh structure, has received considerable attention due to its large accessible surface area, high electrochemical activity, and high electronic conductivity. It also has large abundance and good chemical stability and is a viable candidate in counter electrodes in DSSCs [7–10]. However, graphene aggregates easily due to the intrinsic long-range π-π electronic structure giving rise to small surface area and poor catalytic activity. In order to solve this problem, three-dimensional graphene has been proposed. Yu et al. synthesized vertically-oriented graphene as the counter electrode in DSSCs and the materials showed a charge transfer resistance which is about 1% of Pt and improves the power conversion efficiency of DSSCs [11]. Wang et al. developed a graphene sheet with a 3D honeycomb-like structure which delivered good catalytic performance and energy conversion efficiency [12]. However, there has been seldom research to combine graphene and silicon as the electrode in DSSCs.

The silicon microchannel plate (Si-MCP) is a macro-porous and channel-ordered structure with better properties than conventional porous materials and modification of the Si-MCP inner wall with better electrode materials improves the catalytic performance drastically. In this work, a new nanocomposite electrode based on

* Corresponding authors. College of Communications and Electronics Engineering, Qiqihar University, Heilongjiang, 161006, China.
E-mail addresses: miaofengjuan@163.com (F. Miao), tbr_sir@163.com (B. Tao).
[1] Fengjuan Miao and Rui Miao are common first authors.

http://dx.doi.org/10.1016/j.orgel.2017.02.040
1566-1199/

few-layer graphene supported by 3D silicon MCP is used as the counter electrode in dye-sensitized solar cells. Si-MCP is adopted as the backbone to disperse the few-layer graphene to avoid aggregation and increase the surface-to-volume ratio. The graphene/Si-MCP nanocomposite electrode has a large surface area good chemical stability and the ordered macro-porous structure increases the electrode/electrolyte interfacial area facilitating ion transfer.

2. Experimental details

2.1. Materials and reagents

All the chemical reagents were analytical grade and used as received. Single side polished 100 mm ⟨100⟩ silicon wafers with a resistivity of 2–8 Ω-cm and thickness of 525 μm were used as the starting materials to produce the Si MCPs. Hydrofluoric acid, dimethylformamide, ammonium fluoride, sodium hydroxide, ethanol, and other reagents were used in the reaction. A high-purity graphite rod (6 mm in diameter) was used as the anode, a Pt wire was used as the cathode, and ammonium sulfate was the electrolyte in the two-electrode electrochemical system to produce the few-layer graphene. The aqueous solutions were prepared with 18 MΩ deionized water and all the experiments were carried out at room temperature in a clean environment.

2.2. Preparation of silicon microchannel plates

The Si-MCP was fabricated by traditional microelectronic processing and more details about the fabrication can be found elsewhere [13]. The process included the following main steps: (i) A thick SiO_2 layer was grown thermally on the silicon wafer as a mask; (ii) A proper region was obtained on the front side by photolithography and wet etching in buffered hydrofluoric acid; (iii) Pyramidal notches were created for subsequent anodization; (iv) The SiO_2 layer was remove; (v) Photo-assisted electrochemical etching was performed at a low temperature. The software Labview was employed to control both current densities and etching time.

2.3. Electrochemical exfoliation of graphene from graphite

In the two-electrode system, the distance between the Pt wire and graphite rod was 2.5 cm. The electrolyte was prepared by dissolving 1.06 g of $(NH_4)_2SO_4$ in 80 mL of DI water. The electrochemical exfoliation process was carried out by applying +8 V DC for 30 min. The exfoliated graphene sheets in the suspension was collected with 100 nm porous filter and rinsed with DI water by vacuum filtration. After drying, they were dispersed in the DMF solution under gentle sonication for 15 min [14].

2.4. Fabrication of vertically-oriented few-layer graphene supported by silicon microchannel plate

The Si-MCP was dipped in a solution of Triton X-100 30 **s** to decrease the internal stress and enhance wetting. The graphene solution was stabilized for about 48 h to precipitate un-exfoliated graphite flakes or particles. The top part of the dispersion was used in electrophoresis on the Si-MCP supporter to fabricate the

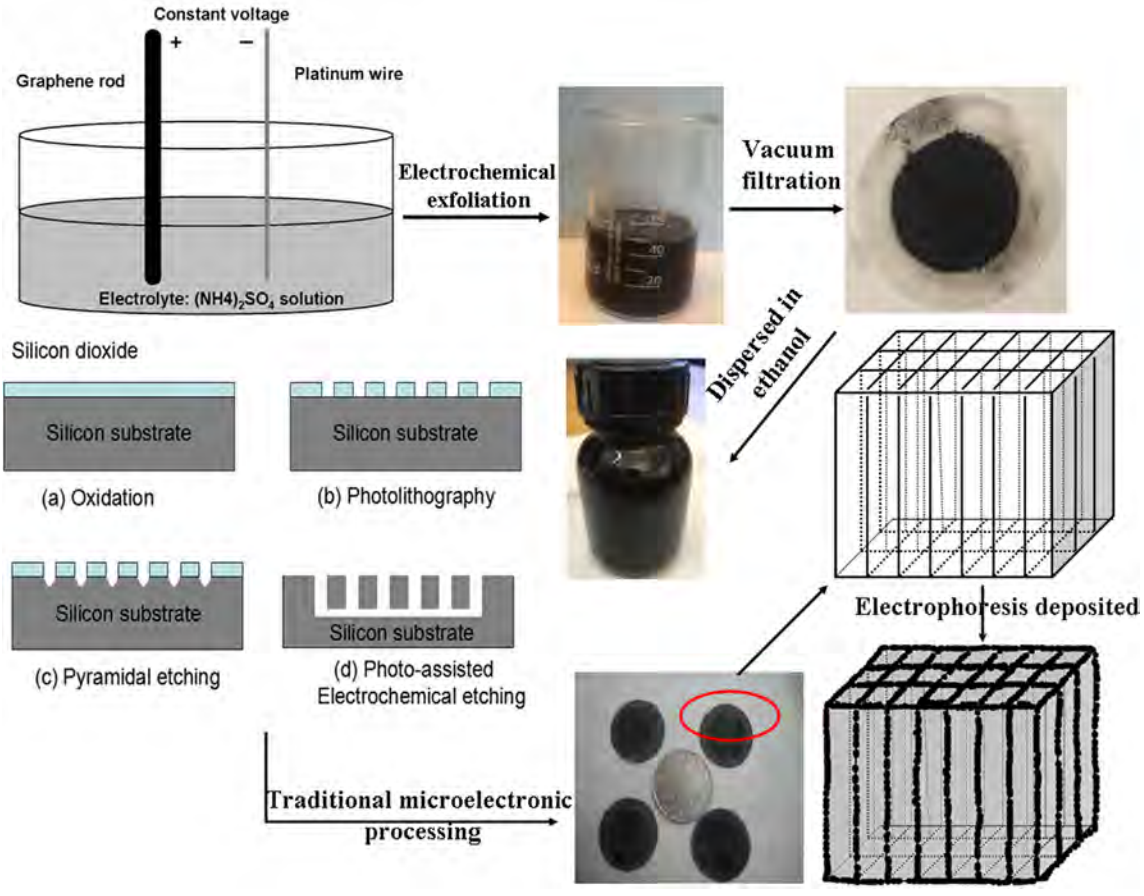

Fig. 1. Fabrication process of the graphene/Si-MCP counter electrode.

graphene/Si-MCP counter electrode. The fabrication process of the graphene/Si-MCP counter electrode is illustrated in Fig. 1. The graphene/Si-MCP samples are annealed under ambient conditions at 300 and 500 °C for 1 h to improve the quality [15–18].

2.5. Characterization

The morphology of the few-layer graphene and graphene/Si-MCP were observed by scanning electron microscopy (SEM). Raman scattering was performed on a dispersive Raman microscope spectrometer with an excitation laser wavelength of 532 nm. The chemical composition and bonding states were determined by x-ray photoelectron spectroscopy (XPS).

2.6. Fabrication of DSSC

The DSSC (active area of 0.25 cm^2) was assembled according to the following procedures. The TiO_2 electrode was obtained by the sol-gel method on the conducting glass substrate sintered at 500 °C for 30 min in air [19]. The TiO_2 photoelectrode was then dipped in a 0.5 mM solution containing the N3 dye and ethanol for 12 h at room temperature. The DSSC was assembled by sandwiching the dye-sensitized nanocrystalline TiO_2 electrode and graphene/Si-MCP counter electrode with a 25 μm thick gap. The electrolyte was introduced into the cell by capillary effects through the thin gap between two electrodes. 0.5 M KI/0.05 M I_2, ethylene carbonate (EC), and propylene carbonate (PC) (EC: PC = 1:4 by volume) were the electrolyte. The photovoltaic performance of the graphene/Si-MCP counter electrode was determined under simulated solar illumination (AM 1.5, 100 mW cm^{-2}) at 25 °C.

3. Results and discussion

As shown in Fig. 2(a), the few-layer graphene has a rumpling and scrolling morphology. Fig. 2(b) and (c) show the representative AFM image and statistical thickness distribution histograms of the graphene nanosheets. The thickness of 80% measured graphene nanosheets is less than 3 nm and the number of layers is less than 5. Based on the statistical analysis, most of the graphene nanosheets have 2–4 layers and the lateral size is between 50 and 650 nm. Fig. 3 displays the image of Si-MCP fabricated by electrochemical etching. It is a connective film having a diameter of 5 μm. The channels have little impurities and are aligned orderly with a depth of approximately 200 μm. The corresponding pictures of the top and cross-sectional SEM images after coverage with graphene are depicted in Fig. 4(a) and (b). The graphene sheets are uniformly distributed on the sidewalls of the silicon MCP and the whole structure remains isolated and parallel to one another. The surface

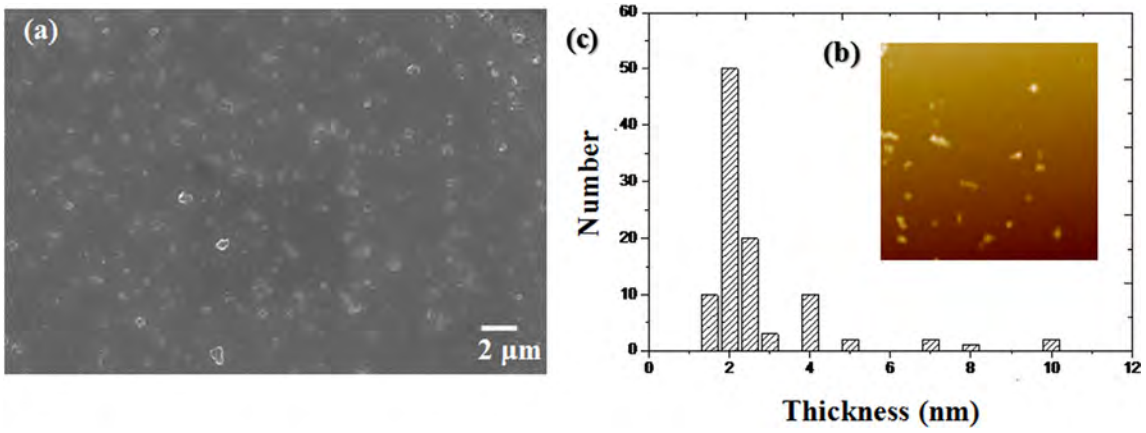

Fig. 2. (a) SEM image of few-layer graphene; (b) AFM image of few-layer graphene; (c) Statistical thickness distribution histograms of the graphene nanosheets.

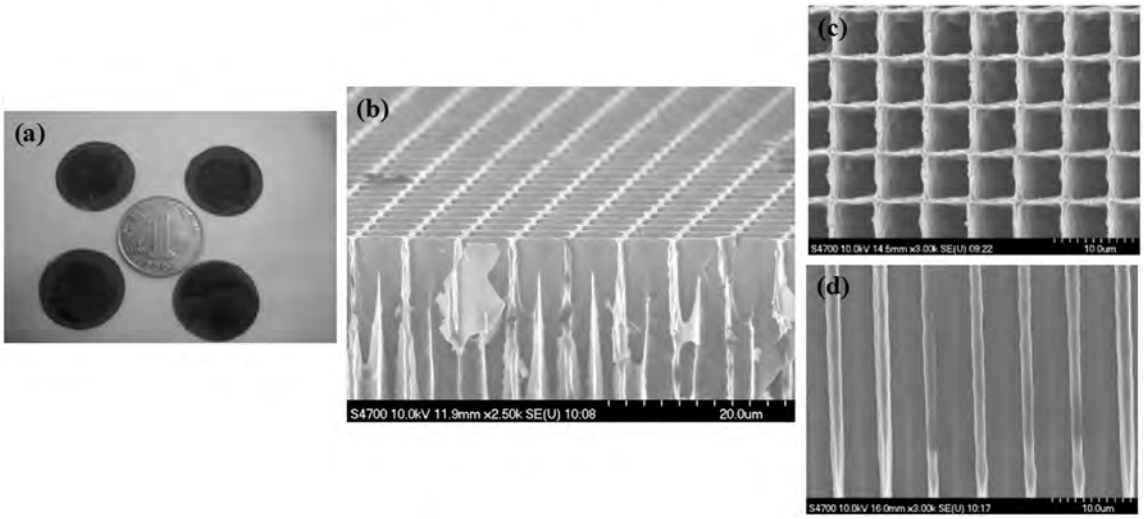

Fig. 3. (a) Photograph of Si-MCP; (b) SEM image of Si-MCP; (c) and (d) Corresponding magnified pictures of the top and cross-section of the Si-MCP.

of the channels becomes rougher. After deposition, there is an additional layer composed of numerous plate-like grains evenly distributed on the outer and inner sidewalls of Si-MCP. The graphene layer consists of many plate-like grains several to hundreds of nanometers in size supported by the Si-MCP producing an ordered graphene/Si-MCP array. The plate-like grains are interconnected and interwined with each other giving rise to a nanoporous graphene/Si-MCP array with a large surface area and short diffusion distance. The microstructure and morphology before and after deposition are similar.

Fig. 4(c) shows the Raman spectra of graphene/Si-MCP, natural graphite, graphene/Si-MCP-300 °C and graphene/Si-MCP-500 °C. The Raman spectra of graphene/Si-MCP shows a clear G-band at 1582 cm^{-1} and 2D band at 2702 cm^{-1}. The 2D band location is different from that of natural graphite (located at 2721 cm^{-1}) and is more intense than that of graphite. The D-band at 1350 cm^{-1} is caused by edge effects and the intensity of the G peak is not much larger than that of the D peak, indicating there are more defects which may favor application. The higher relative intensity and the decreased Raman frequency shifts of the 2D band indicate decreased graphene layers as consistent with AFM. After annealing at 300 °C, the D band decreases and the G peak is larger than the D peak while the 2D band is still absent. After annealing at 500 °C, the D band is again intense but the 2D band is still absent similar to graphene oxide. Fig. 4(d) shows the X-ray photoelectron spectroscopy (XPS) spectra of the graphene/Si-MCP, graphene/Si-MCP-300 °C, and graphene/Si-MCP-500 °C. The C1s and O1s signals are observed at 284 and 530 eV and the oxygen content in graphene/Si-MCP-300 °C is the smallest among the three samples. Fig. 4(e) presents the high-resolution C1s spectra of graphene/Si-MCP, graphene/Si-MCP-300 °C, and graphene/Si-MCP-500 °C, which can be fitted with three Gaussian peaks at 284.1, 285.5, and 288.0 eV

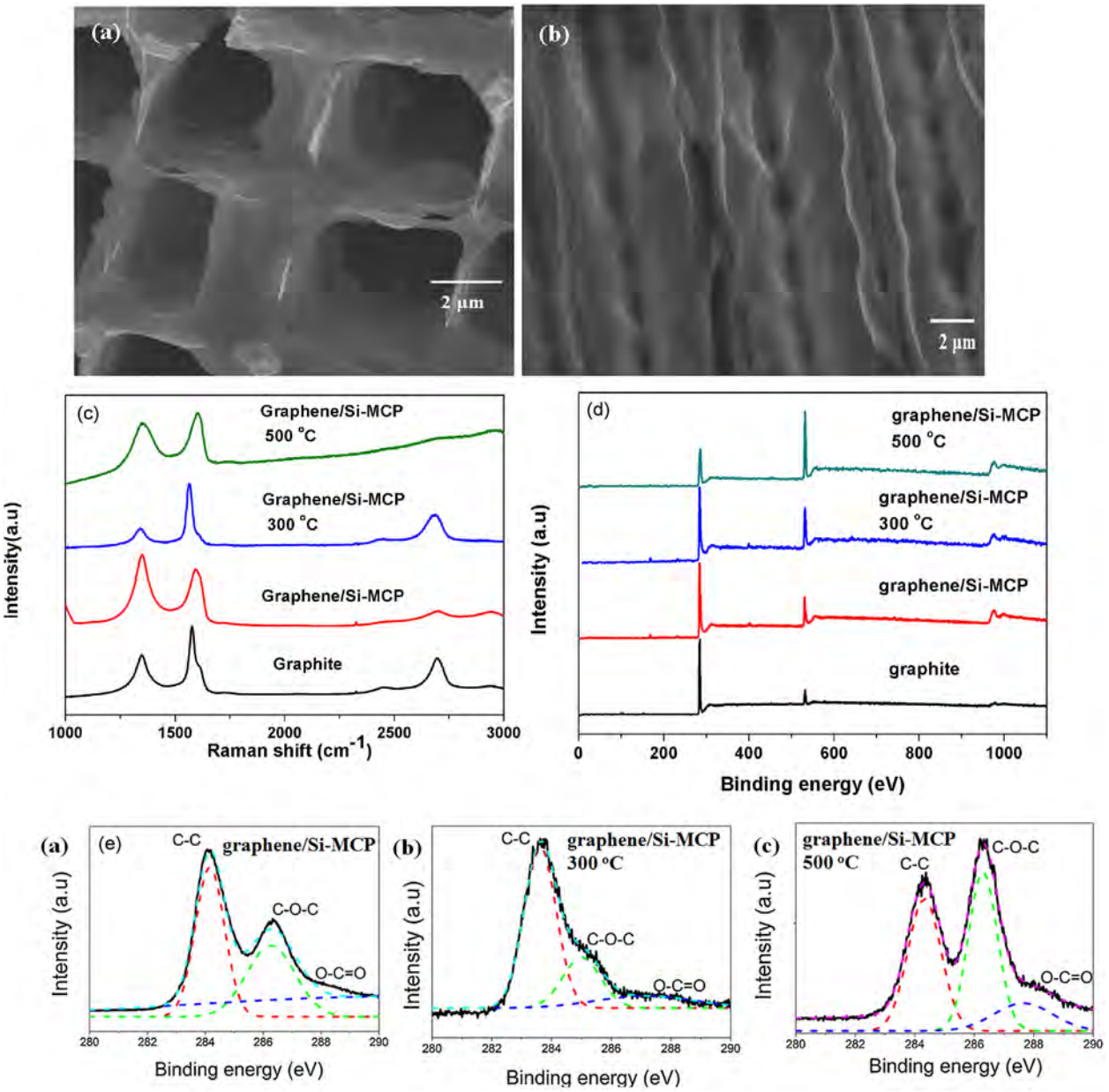

Fig. 4. (a) and (b) Top and cross-sectional SEM images of graphene/Si-MCP; (c) Raman scattering spectra of graphene/Si-MCP, graphene/Si-MCP-300 °C, and graphene/Si-MCP-500 °C; (d) X-ray photoelectron spectroscopy (XPS) spectra of graphene/Si-MCP, graphene/Si-MCP-300 °C, and graphene/Si-MCP -500 °C; (e) High-resolution C1s spectra of graphene/Si-MCP, graphene/Si-MCP-300 °C, and graphene/Si-MCP-500 °C.

attributed to sp^2 C (C–C,C=C), sp^3 C(C–O), and oxidized C (C=O), respectively. Graphene/Si-MCP shows a strong peak of C=C suggestion good graphitization and the absence of oxygen-containing functional groups. After annealing at 300 °C for 1 h, the sample exhibits a strong peak for oxidized C and the peak intensity decreases substantially indicating that the amount of oxygen-containing functional groups is significantly reduced after the thermal treatment. After annealing at 500 °C, the amount of oxygen-containing functional groups increases giving rise to graphene oxide.

Cyclic voltammetry (CV) is conducted to analyze the reaction kinetics of the I^-/I_3^- couple on the counter electrode. Fig. 5 show the CVs of the counter electrodes of graphene/Si-MCP, graphene/Si-MCP-300 °C, and graphene/Si-MCP-500 °C at a scanning rate of 50 mV s^{-1}. Two pairs of redox peaks are observed. The one at the low potential can be attributed to the redox reaction in reaction (1) and that at the high potential to reaction (2) [20] as shown in the following:

$$I_3^- + 2e^- \leftrightharpoons 3I^- \text{ and} \quad (1)$$

$$3I_2 + 2e^- \leftrightharpoons 2I_3^-. \quad (2)$$

The peak current and peak-to-peak separation (ΔE_p) are two important parameters to comparing the catalytic activity of different counter electrodes. The larger the peak current density and the smaller the ΔE_p value, the better is the catalytic activity. Graphene/Si-MCP-300 °C shows the largest current density and smallest ΔE_p. The increase in the peak current density in triiodide reduction indicates good elecrocatalytic activity towards reduction of I_3^- to I^-. According to Nicholson, ΔE_p varies inversely with the charge transfer rate (k_s, electrochemical rate constant of the redox reaction) and so the minimum ΔE_p indicates the highest k_s [21]. The larger peak current density and smaller ΔE_p reveal that graphene/Si-MCP-300 °C is a better choice for reduction of I_3^-. The CV curves of graphene/Si-MCP annealed at 300 °C in the I^-/I_3^- system at different scanning rates are shown in Fig. 6 and the inset illustrates the dependence of the current density of the I^-/I_3^- reduction peaks to the scanning rate. The linear relationship between the redox peak current density and square root of the scanning rate indicates that it is a controlled by ion diffusion in the electrolyte and may be related to the transport of the I^-/I_3^- couple away from the graphene/Si-MCP-300 °C electrode surface, further implying easy penetration and diffusion as well as a large number of reduction sites on the graphene/Si-MCP-300 °C structure.

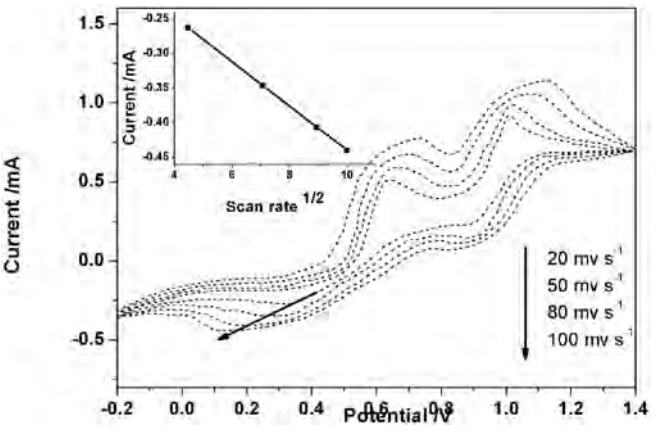

Fig. 6. Cyclic voltammograms of graphene/Si-MCP-300 °C in the I^-/I_3^- system at different scanning rates (Inset: Dependence of the current density of the I^-/I_3^- reduction peaks on the scanning rate).

Fig. 7 presents the electrochemical impedance spectroscopy (EIS) characteristics of the graphene/Si-MCP-300 °C counter electrodes. Usually, the impedance at low frequencies corresponds to Nernst diffusion of I^-/I_3^- in the electrolyte, whereas that at high frequencies is associated with the capacitance and charge-transfer resistance at the electrode-electrolyte interface. The medium frequency response is related to the photoelectrode-dye-electrolyte interface where accumulation of photoelectrons and redox shuttles is expected [22–24]. The equivalent circuit to fit the EIS data is shown in the inset in Fig. 7. The resistance element R_s in the high-frequency region can be ascribed to the sheet resistance of the substrate, R_{ct} is a charge transfer resistance, C is the capacitance of double electrical layer, and Warburg impedance (W) is related to the Nernst diffusion of redox species in the electrolyte.

In general, the quality of the catalytic electrode is characterized by the charge transfer resistance at the electrolyte/counter electrode interface, R_{ct} and it varies inversely with the current density, j_0:

$$j_o = \frac{RT}{nFR_{CT}}. \quad (3)$$

In this relationship, R is the universal gas constant, T is the

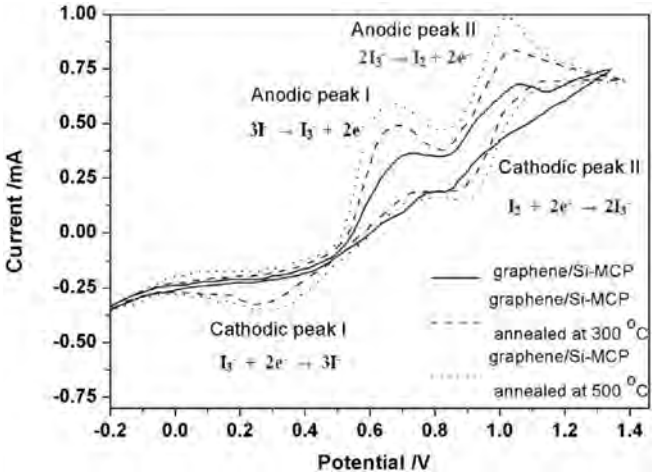

Fig. 5. Cyclic voltammograms of the counter electrodes composed of graphene/Si-MCP-300 °C and graphene/Si-MCP-500 °C at a scanning rate of 50 mV s^{-1}.

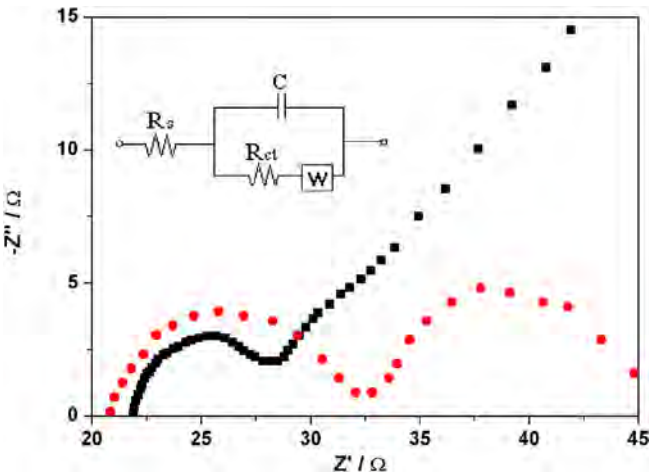

Fig. 7. Electrochemical impedance spectroscopy (EIS) characteristics of the graphene/Si-MCP and graphene/Si counter electrodes.

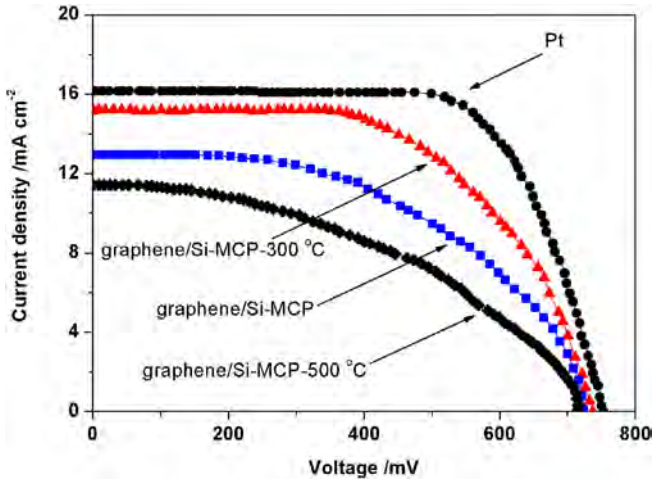

Fig. 8. Photocurrent-voltage (J-V) characteristics of the DSSCs composed of the graphene/Si-MCP and graphene/Si counter electrodes.

Table 1
Photoelectric parameters of DSSCs comprising the graphene/Si-MCP counter electrodes after annealing at different temperature.

Sample	J_{sc} (mA cm^{-2})	V_{oc} (mV)	FF	η
Pt	16.13	751.18	0.68	8.30%
graphene/Si-MCP	12.98	725.22	0.58	5.46%
graphene/Si-MCP-300 °C	15.18	737.43	0.64	7.16%
graphene/Si-MCP-500 °C	11.40	712.84	0.50	4.06%

absolute temperature, F is the Faraday constant, and n is the stoichiometric number of electrons involved in the reaction. A smaller R_{ct} implies more efficient electron exchange at the interface of the electrolyte. As shown Fig. 7, R_{ct} of graphene/Si-MCP-300 °C is 7.8 Ω and it is similar to that of the FTO/Pt electrode (11.39 Ω). R_{ct} of graphene/Si-MCP-300 °C is smaller than that of the Pt counter electrode showing high electrocatalytic activity [25–28].

Fig. 8 shows the photocurrent-voltage (J-V) characteristics of the DSSCs composed of the graphene/Si-MCP, graphene/Si-MCP-300°, and graphene/Si-MCP-500 °C counter electrodes. Table 1 shows the corresponding data from the current-voltage characteristics under simulated solar irradiation (AM 1.5G, 100 mW cm^{-2}). For the DSSC fabricated with graphene/Si-MCP-300 °C counter electrode, the open circuit voltage (Voc), current density (Jsc), fill factor (FF), and conversion efficiency (η) are 737.43 mV, 15.18 mA-cm^{-2}, 0.64, and 7.16%, respectively. The current density of graphene/Si-MCP-300 °C is the larger than those of graphene/Si-MCP and graphene/Si-MCP-500 °C.

4. Conclusion

An ordered graphene/Si-MCP counter electrode is prepared by conventional microelectronics fabrication techniques and electrophoresis. The graphene/Si-MCP with a large surface area and defect-rich surface shows a small charge transfer resistance and delivers excellent photovoltaic performance. Owing to the microelectronics-compatible fabrication process, the materials have large potential in commercial energy storage devices.

Acknowledgements

This work was jointly supported by the National Natural Science Foundation of China (Grant Nos. 61204127, 81172204 and 81271628), Natural Science Foundation of Heilongjiang Province (Grant No. F201332, F201438), Postdoctoral scientific research developmental fund of Heilongjiang Province (Grant No. LBH-Q15142, LBH-Q14157), New Century Excellent Talents In Heilongjiang Provincial University (Grant No. 1253-NECT025), Science and Technology Project of Qiqihar (Grant GYGG-201409), Higher school science and technology achievements industrialization pre-research and development Foundation of Heilongjiang Province (Grant No. 1254CGZH04) and City University of Hong Kong Applied Research Grant (ARG) No. 9667122.

References

[1] B. O'Regan, M. Gratzel, A low-cost, high-efficiency solar cell based on dye-sensitized colloidal TiO_2 films, Nature 353 (1991) 737.
[2] M. Grätzel, Solar energy conversion by dye-sensitized photovoltaic cells, Inorg. Chem. 44 (2005) 6841.
[3] A. Yella, H.-W. Lee, H.N. Tsao, C. Yi, A.K. Chandiran, M.K. Nazeeruddin, E.W.-G. Diau, C.-Y. Yeh, S.M. Zakeeruddin, M. Grätzel, Porphyrin-sensitized solar cells with cobalt (II/III)–Based redox electrolyte exceed 12 percent efficiency, Science 334 (2011) 629.
[4] C.H. Tsai, S.Y. Hsu, C.Y. Lu, Y.T. Tsai, T.W. Huang, Y.F. Chen, Y.H. Jhang, C.C. Wu, A novel amine-free dianchoring organic dye for efficient dye-sensitized solar cells, Org. Electron 13 (2012) 199.
[5] A. Hauch, A. Georg, Diffusion in the electrolyte and charge-transfer reaction at the platinum electrode in dye-sensitized solar cells, Electrochim. Acta 46 (2001) 3457.
[6] C.Y. Chen, M.K. Wang, J.Y. Li, et al., Antibunching single-photon emission and blinking suppression of CdSe/ZnS quantum dots, ACS Nano 3 (2009) 3103.
[7] H. Wang, Y.H. Hu, Graphene as a counter electrode material for dye-sensitized solar cells, Energy Environ. Sci. 5 (8) (2012) 8182.
[8] D. Zhang, X. Li, H. Li, S. Chen, Z. Sun, X. Yin, et al., Graphene based counter electrode for dye-sensitized solar cells, Carbon 49 (15) (2011) 5382.
[9] Y. Xue, J. Liu, H. Chen, R. Wang, D. Li, J. Qu, et al., Nitrogen-doped graphene foams as metal-free counter electrodes in highperformance dye-sensitized solar cells, Angew. Chem. Int. Ed. 51 (48) (2012) 12124.
[10] J. Liu, Y. Xue, M. Zhang, L. Dai, Graphene-based materials for energy applications, MRS Bull. 37 (12) (2012) 1265.
[11] K. Yu, Z. Wen, H. Pu, G. Lu, Z. Bo, H. Kim, Y. Qian, E. Andrew, S. Mao, J. Chen, Hierarchical vertically oriented graphene as a catalytic counter electrode in dye-sensitized solar cells, J. Mater. Chem. A 1 (2013) 188.
[12] H. Wang, K. Sun, F. Tao, D.J. Stacchiola, Y.H. Hu, 3D honeycomb-like structured graphene and its high efficiency as a counter-electrode catalyst for dye-sensitized solar cells, Angew. Chem. Int. Ed. 52 (2013) 9210.
[13] X.M. Chen, J.L. Lin, D. Yuan, P.L. Ci, P.S. Xin, S.H. Xu, L.W. Wang, Obtaining a high area ratio free-standing silicon microchannel plate via a modified electrochemical procedure, J. Micromechan. Microeng. 18 (3) (2008) 037003.
[14] K. Parvez, Z.S. Wu, R.J. Li, X.J. Liu, R. Graf, X.L. Feng, Exfoliation of graphite into graphene in aqueous solutions of inorganic salts, J. Am. Chem. Soc. 136 (2014) 6083.
[15] F.J. Miao, S. Majee, M. Song, J. Zhao, S.L. Zhang, Z.B. Zhang, Inkjet printing of electrochemically-exfoliated graphene nano-platelets, Synth. Met. 220 (2016) 318.
[16] X.F. Song, D.P. Wei, T. Sun, A stably enhanced transparent conductive graphene film obtained using an air- annealing method, Mater. Res. Express 3 (2016) 085003.
[17] J.C. Chou, C.H. Huang, Y.J. Lin, The Influence of different annealing temperatures on graphene modified TiO_2 for dye-sensitized solar cell, IEEE Trans. Nanotechnol. 15 (2016) 164.
[18] S. Majee, M. Song, S.L. Zhang, Z.B. Zhang, Scalable inkjet printing of shear-exfoliated graphene transparent conductive films, Carbon 102 (2016) 51.
[19] B.R. Tao, F.J. Miao, J.H. Chu, Structure and photoelectrochemical properties of silicon microstructures arrays, Electrochim. Acta 108 (2013) 248.
[20] P. Joshi, L. Zhang, Q. Chen, D. Galipeau, H. Fong, Q. Qiao, Electrospun carbon nanofibers as low-cost counter electrode for dye-sensitized solar cells, ACS Appl. Mater. Interfaces 2 (2010) 3572.
[21] R.S. Nicholson, Theory and application of cyclic voltammetry for measurement of electrode reaction kinetics, Anal. Chem. 37 (1965) 1351.
[22] L. Kavan, J.H. Yum, M. Gratzel, Optically transparent cathode for dye-sensitized solar cells based on graphene nanoplatelets, Acs Nano 5 (2011) 165.
[23] L.Y. Han, N. Koide, Y. Chiba, A. Islam, R. Komiya, N. Fuke, A. Fukui, R. Yamanaka, Improvement of efficiency of dye-sensitized solar cells by reduction of internal resistance, Appl. Phys. Lett. 86 (2005) 213501.
[24] S. Phadke, A.D. Pasquier, D.P. Birnie, Enhanced electron transport through template-derived pore channels in dye-sensitized solar cells, J. Phys. Chem. C 115 (2011) 18342.
[25] F. Xu, J. Chen, X. Wu, Y. Zhang, Y. Wang, J. Sun, H. Bi, W. Lei, Y. Ni, L.T. Sun, Graphene scaffolds enhanced photogenerated electron transport in ZnO photoanodes for high-efficiency dye-sensitized solar cells, J. Phys. Chem. C 117 (2013) 8619.
[26] L.S. Zhu, J. Zhang, X.W. Xu, Y.Z. Yu, X. Wu, T. Yang, X.H. Wang, Room

temperature H2 detection based on Pd/SiNWs/p-Si Schottky diode structure, Sensors Actuators B Chem. 227 (2016) 515.
[27] F.J. Miao, B.R. Tao, P.L. Ci, J. Shi, L.W. Wang, P. Chu, 3D ordered NiO/silicon MCP array electrode materials for electrochemical Supercapacitors, Mater. Res. Bull. 44 (2009) 1920.
[28] B.R. Tao, J. Zhang, F.J. Miao, S.C. Hui, L.J. Wan, Preparation and electrochemistry of NiO/SiNW nanocomposite electrodes for electrochemical capacitors, Electrochim. Acta 55 (2010) 5258.